Anal. Chem. **2007,** *79,* 7027−7035

Employing Two Different Quartz Crystal Microbalance Models To Study Changes in Viscoelastic Behavior upon Transformation of Lipid Vesicles to a Bilayer on a Gold Surface

Nam-Joon Cho,[†,‡] Kay K. Kanazawa,[‡] Jeffrey S. Glenn,[§] and Curtis W. Frank*[,‡]

Departments of Materials Science and Engineering and Chemical Engineering, Department of Chemical Engineering, and Department of Medicine, Division of Gastroenterology and Hepatology, Stanford University School of Medicine, Stanford University, Stanford, California 94305

By analyzing the viscoelastic properties of two distinct layers, a layer of "soft" vesicles and a "rigid" bilayer, we have created a model system to permit the study of film behavior in the region of nonlinear mass and frequency change (non-Sauerbrey). The structural transformation of lipid vesicles to a bilayer is shown to be accompanied by significant changes in their physical properties. After the adsorption and saturation of intact vesicles on gold surfaces, the adsorbed vesicle layer exhibits a soft, water−rich, viscoelastic state. The AH peptide, a vesicle-destabilizing agent, is then added to trigger the formation of a much thinner (∼5 nm), compact, and rigid bilayer. In this study, we used the quartz crystal microbalance with dissipation technique. Large non-Sauerbrey frequency and energy dissipation changes characterize the viscoelastic nature of adsorbed intact vesicle films thicker than ∼10 nm. Once the transformation is complete, the frequency changes along with zero energy dissipation for sufficiently thin films ($t \sim 5$ nm) were effectively modeled with the Sauerbrey equation. Furthermore, we checked the validity of the Voigt−Voinova model in which the quartz substrate is treated as a Voigt element, which is beyond the Sauerbrey description. The calculations treating the film as having a constant viscosity agreed well with the Voigt−Voinova model. These results were compared to calculations done using the electromechanical (EM) model, which does not require a series expansion. The Voigt−Voinova results were in excellent agreement with the EM model, providing evidence that the expansion used in their study is quite accurate.

In emerging scientific applications of lipid−peptide interactions, e.g., binding dynamics, adsorption−desorption, and molecular affinity, researchers have relied on surface-based analytical techniques. The quartz crystal microbalance (QCM) technique is sensitive to the mass changes as well as the viscoelastic properties of an adsorbed film.[1−4] It has been widely utilized in nanorange mass detection systems due to its high precision, high sensitivity, reliability, simplicity of measurement, ease of analysis, and convenience as a tool for real-time measurements of macromolecule interactions in several liquid-state research applications.[5−12] The most commonly used applications are in bioscience and electrochemistry.[5−13] It has proved to be a valuable instrument for the study of membrane-bound proteins,[14−16] membrane-mediated cellular processes,[17−23] protein−lipid interactions,[21,22,24−27]

* To whom correspondence should be addressed. E-mail: curt.frank@stanford.edu.

[†] Departments of Materials Science and Engineering and Chemical Engineering.

[‡] Department of Chemical Engineering.

[§] Department of Medicine.

(1) Lucklum, R.; Behling, C.; Cernosek, R. W.; Martin, S. J. *J. Phys. D: Appl. Phys.* **1997**, *30*, 346−356.
(2) Frye, G. C.; Martin, S. J. *Appl. Spectrosc. Rev.* **1991**, *26*, 73−149.
(3) Brown, M. J.; Hillman, A. R.; Martin, S. J.; Cernosek, R. W.; Bandey, H. L. *J. Mater. Chem.* **2000**, *10*, 115−126.
(4) Bandey, H. L.; Martin, S. J.; Cernosek, R. W.; Hillman, A. R. *Anal. Chem.* **1999**, *71*, 2205−2214.
(5) Keller, C. A.; Glasmastar, K.; Zhdanov, V. P.; Kasemo, B. *Phys. Rev. Lett.* **2000**, *84*, 5443−5446.
(6) Keller, C. A.; Kasemo, B. *Biophys. J.* **1998**, *75*, 1397−1402.
(7) Knoll, W. *Annu. Rev. Phys. Chem.* **1998**, *49*, 569−638.
(8) Kanazawa, K. K.; Reed, C. E. *Abstr. Pap. Am. Chem. Soc.* **1989**, *198*, 89-Anyl.
(9) Kanazawa, K. K. *J. Electroanal. Chem.* **2002**, *524*, 103−109.
(10) Hook, F.; Rodahl, M.; Brzezinski, P.; Kasemo, B. *J. Colloid Interface Sci.* **1998**, *208*, 63−67.
(11) Hook, F.; Kasemo, B.; Nylander, T.; Fant, C.; Sott, K.; Elwing, H. *Anal. Chem.* **2001**, *73*, 5796−5804.
(12) Li, J.; Wu, Z. Y.; Xiao, L. T.; Zeng, G. M.; Huang, G. H.; Shen, G. L.; Yu, R. Q. *Anal. Sci.* **2002**, *18*, 403−407.
(13) Marx, K. A. *Biomacromolecules* **2003**, *4*, 1099−1120.
(14) Sato, T.; Serizawa, T.; Okahata, Y. *Biochim. Biophys. Acta* **1996**, *1285*, 14−20.
(15) Ross, M.; Gerke, V.; Steinem, C. *Biochemistry* **2003**, *42*, 3131−3141.
(16) Sellborn, A.; Andersson, M.; Hedlund, J.; Andersson, J.; Berglin, M.; Elwing, H. *Mol. Immunol.* **2005**, *42*, 569−574.
(17) Steinem, C.; Janshoff, A.; Wegener, J.; Ulrich, W. P.; Willenbrink, W.; Sieber, M.; Galla, H. J. *Biosens. Bioelectron.* **1997**, *12*, 787−808.
(18) Langford, J.; Pavey, K. D.; Olliff, C. J.; Cragg, P. J.; Hanlon, G. W.; Paul, F.; Rees, G. D. *Analyst* **2002**, *127*, 360−367.
(19) Sota, H.; Yoshimine, H.; Whittier, R. F.; Gotoh, M.; Shinohara, Y.; Hasegawa, Y.; Okahata, Y. *Anal. Chem.* **2002**, *74*, 3592−3598.
(20) Ciolczyk-Wierzbicka, D.; Amoresano, A.; Casbarra, A.; Hoja-Lukowicz, D.; Litynska, A.; Laidler, P. *Glycoconjugate J.* **2004**, *20*, 483−492.
(21) Li, J.; Thielemann, C.; Reuning, U.; Johannsmann, D. *Biosens. Bioelectron.* **2005**, *20*, 1333−1340.
(22) Hianik, T.; Ostatna, V.; Zajacova, Z.; Stoikova, E.; Evtugyn, G. *Bioorg. Med. Chem. Lett.* **2005**, *15*, 291−295.
(23) Richter, R. P.; Brisson, A. R. *Biophys. J.* **2005**, *88*, 3422−3433.

10.1021/ac0709504 CCC: $37.00
Published on Web 08/08/2007

cell−cell interactions,[28,29] antibody−antigen interactions,[21,22,24−27] biological signal transduction,[12,30] and drug delivery detection.[13,19,31]

A valuable advantage of the QCM technique for thin films is its capability to detect an adsorbed mass, Δm, in the nanogram range, using a linear relationship between the added mass and the change in resonant frequency, as described by Sauerbrey.[32] Based on the assumption of a homogeneous foreign mass with a spatially uniform density, the famous Sauerbrey equation,[32] written to include harmonic resonances, is

$$\Delta m = -C_{\mathrm{QCM}}(\Delta f_n/n) \qquad (1)$$

where Δm is the adsorbed mass on the surface, C_{QCM} is the mass sensitivity constant (17.7 ng·cm^{-2}·Hz^{-1} at $f = 5$ MHz), and Δf_n is the change in the resonance frequency at the nth harmonic. The harmonic order n has values (1,3,5,...). C_{QCM} is a constant independent of the harmonic order n. If the Sauerbrey relation is satisfied, then the normalization of the observed frequency change at the nth harmonic by n should yield a constant value. If an ideal mass rigid layer is assumed, eq 1 has been demonstrated to provide an accurate modeling fit, as seen in previous research on lipid monolayers, bilayers, or hexadecanethiols adsorbed on solid substrates.[5,6,10] One can use the normalized frequency changes at the harmonics to test for the validity of the Sauerbrey relation. For sufficiently "soft" layers, however, the Sauerbrey equation does not fit the data well.

As Höök[11] and Voinova[33] have described, two reasons explain the deviations from the Sauerbrey relation. One reason is that the adlayer may be viscoelastic, as in the case of adsorbed vesicles, which gives rise to a compound resonator for which Δf is not directly proportional to Δm.[11] In this case, the frequency change becomes sensitive to the mechanical properties of the film, including the shear modulus and viscosity. The other reason is that the molar mass (or dry mass) by itself is insufficient to describe the film mass. The mass of water, associated with the film, must also be included. For vesicle adsorption on a gold surface that results in a soft layer, the water may appear to contribute to the mass increase due to direct hydration, coupling between vesicles, or entrapment on a roughened surface. In other words, the additional mass of water between the vesicles is recognized as a part of the adsorbed layer and contributes to the viscoelastic behavior. The typical amount of coupled water has been shown to vary significantly in different systems depending on the nature of the film, with estimations of mass uptake ranging from 1.5 to 10 times larger than the molar mass of the adsorbed material.[11]

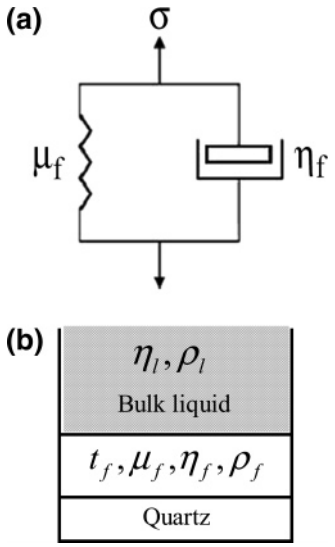

Figure 1. Voigt−Voinova model system used to analyze viscoelastic properties. (a) The film is subject to an oscillating shear stress, σ, and behaves like a Voigt element with shear viscosity, η_f, and shear modulus, μ_f. (b) Schematic illustration of the geometry of a QCM covered by a film with a thickness, t_f, in contact with a semi-infinite Newtonian liquid.

In the present study, the interpretation of physical properties of the adsorbed film is based on the model presented by Voinova et al.[34] In addition, these results were compared to calculations done using the electromechanical (EM) model,[8,35] which does not require a series expansion. In the Voigt−Voinova model, the adsorbed film is represented by a single Voigt element (Figure 1a), the quartz crystal is assumed to be purely elastic, and the surrounding solution is assumed to be purely viscous and Newtonian. Further, it is assumed that the thickness, t_f, and the density, ρ_f, of the film are uniform, that the viscoelastic properties of shear modulus and viscosity are frequency independent, and that there is no slip between the adsorbed layer and the crystal during shearing. The adsorbed layer is represented with a homogeneous film on the sensor surface using four unknown parameters (ρ_f, t_f, μ_f, η_f). Above the adsorbed film is a semi-infinite bulk liquid (ρ_l, η_l), as illustrated in Figure 1b.

We first employed the Voigt−Voinova model to evaluate the experimentally measured Δf and ΔD for the bound mass in order to gain insight into the structural changes of the adsorbed film on the solid support. The adsorbed layer is represented by a frequency-dependent complex shear modulus, which is defined by

$$G = G' + iG'' = \mu_f + 2\pi i f \eta_f = \mu_f\,(1 + 2\pi i f \tau_f) \qquad (2)$$

where G' describes energy storage, G'' describes energy dissipation, f is the oscillation frequency, μ_f is the elastic shear (storage) modulus, η_f is the shear viscosity (loss modulus), and τ_f is the characteristic relaxation time of the film ($\tau_f = \eta_f/\mu_f$). The

(24) Ohtsuka, K.; Kajiki, R.; Waki, M.; Nojima, T.; Takenaka, S. *Analyst* **2004**, *129*, 888−889.
(25) Mascini, M.; Macagnano, A.; Monti, D.; Del Carlo, M.; Paolesse, R.; Chen, B.; Warner, P.; D'Amico, A.; Di Natale, C.; Compagnone, D. *Biosens. Bioelectron.* **2004**, *20*, 1203−1210.
(26) Wang, Z.; Zhang, L.; Lu, J. *J. Mol. Model (Online)* **2005**, *11*, 80−86.
(27) Ersoz, A.; Denizli, A.; Ozcan, A.; Say, R. *Biosens. Bioelectron.* **2005**, *20*, 2197−2202.
(28) Redepenning, J.; Schlesinger, T. K.; Mechalke, E. J.; Puleo, D. A.; Bizios, R. *Anal. Chem.* **1993**, *65*, 3378−3381.
(29) Gryte, D. M.; Ward, M. D.; Hu, W. S. *Biotechnol. Prog.* **1993**, *9*, 105−108.
(30) Fung, Y. S.; Wong, Y. Y. *Anal. Chem.* **2001**, *73*, 5302−5309.
(31) Marx, K. A.; Zhou, T.; Montrone, A.; Schulze, H.; Braunhut, S. J. *Biosens. Bioelectron.* **2001**, *16*, 773−782.
(32) Sauerbrey, G. *Z. Phys.* **1959**, *155*, 206−222.
(33) Voinova, M. V.; Jonson, M.; Kasemo, B. *Biosens. Bioelectron.* **2002**, *17*, 835−841.
(34) Voinova, M. V.; Rodahl, M.; Jonson, M.; Kasemo, B. *Phys. Scr.* **1999**, *59*, 391−396.
(35) Kanazawa, K. K. *Faraday Discuss.* **1997**, 77−90.

governing viscoelastic functions for the Voigt element are defined using these variables. The adsorbed film is considered to have a uniform thickness, t_f, and a uniform density, ρ_f. In this viscoelastic model, the adsorbed film is represented by a single Voigt element, consisting of a spring that corresponds to the shear rigidity and a dashpot that represents viscosity, as shown in Figure 1a.

THEORY

Quartz Crystal Microbalance-Dissipation (QCM-D) Modeling. The adsorption kinetics and properties of the adsorbed layer were studied using the QCM-D technique (Q-Sense AB), described in detail elsewhere.[36] It allows concurrent measurements of Δf and ΔD at the first, third, etc., overtone ($n = 1, 3,...$; i.e., $f =$ 5 MHz, 15 MHz,...) up to $n = 7$, to obtain the resonant frequencies, $f_{n=1}, f_{n=3}$, etc., and the corresponding dissipation values, $D_{n=1}$, $D_{n=3}$, etc., with a repetition rate of ~1 Hz. Since the linear relationship between the adsorbed mass and the change in frequency (eq 1) is not necessarily valid for viscoelastic films, which exhibit additional energy dissipations as well as frequency (overtone)-dependent responses, this type of information is very important in understanding complex biomembrane research.[5,6] This is because if the system under investigation exhibits frequency and dissipation dependence in the measured interval (5−35 MHz in our case), measurements at several harmonics will allow the set of data (at $n = 1, 3, 5, 7$) to be compared with the theoretical representations (with several unknown parameters) that must be applied in such situations.

The Voigt−Voinova model includes these viscoelastic effects and assumes uniform thickness, uniform film density, liquid with Newtonian characteristics, and no slip. Further, it is assumed that the film viscosity is independent of overtone frequencies. Then, Δf and ΔD can be related to the film density, viscoelastic properties, and thickness in terms of a Taylor expansion:[34]

$$\Delta_f \cong \frac{1}{2\pi\rho_q t_q} t_f \rho_f \omega\left(1 + \frac{2t^2\chi}{3\delta^2(1+\chi^2)}\right) \quad (3)$$

$$\Delta D \cong \frac{2t^3 \rho_f f}{3\pi f_{ro}\rho_q t_q} \frac{1}{\delta^2 (1+\chi^2)} \quad (4)$$

$$\tan\delta = \frac{1}{\chi} = \frac{2\pi f\eta_f}{\mu_f} \quad (5)$$

$$\delta_{Voigt} = \sqrt{2\eta_f/\rho_f f} \quad (6)$$

where and are the density of the quartz and film, respectively; t_q and t_f are the thickness of the quartz and film, respectively; f is the measured frequency; χ is the inverse of the mechanical loss tangent (tan δ) and is the ratio of the storage modulus (μ_f) and the loss modulus (η_f); f_{ro} is the resonance frequency of the crystal; and δ_{Voigt} is a descriptor for the viscous penetration depth. This viscous penetration depth, or decay length, of the shear wave influences the degree to which the film affects the frequency and dissipation changes. For the general viscoelastic case, the decay length can be determined from the complex acoustic wavevector k, given by the relation

$$k = \omega\sqrt{\rho_f/G} \quad (7)$$

The decay length is the inverse of the imaginary part of k. It is possible to express the decay length using the following expression (8), which we used in our calculations,

$$\delta = \frac{2(\mu_F^2 + \omega^2\eta_F^2)}{\rho_F\omega^2\eta_F}\sqrt{\frac{\rho_F}{2(\mu_F^2 + \omega^2\eta_F^2)}(\mu_F + \sqrt{\mu_F^2 + \omega^2\eta_F^2})} \quad (8)$$

Voinova et al. defined δ_{Voigt} to be the penetration depth for general viscoelastic materials, which includes non-Newtonian liquids. Using four different overtones and eqs 3 and 4, we fit changes in the frequency and dissipation to the film viscosity (η_f), shear modulus (μ_f), thickness (t_f), and density (ρ_f). Overtones were fitted to this model using the commercial program Q-tools software (Q-Sense AB).

This article relies on our previous work[37] in which we introduced a novel method by which the amphipathic α-helical (AH) peptide (Figure 2) was used to destabilize the adsorbed vesicle, leading to lipid bilayer formation on a solid gold substrate. We show the AH and nonamphipathic nonhelical peptides (NH) peptides of the HCV nonstructural protein, NS5A in Figure 2. The amphipathic nature of the helix (indicated by the blue hydrophobic continuous band) is extended in the AH peptide (Figure 2). The NH peptide, however, is synthesized with three-point mutations introduced into the AH to disrupt amino acids on the hydrophobic face. Three charged amino acids (pink) were spaced at intervals along the predicted N-terminal α -helix such that no sustained hydrophobic patch remained. The length of the peptide is 46 Å and the largest width is 20 Å as estimated using the Hyperchem program. These measurements are based on a perfect helix using average bond lengths and angles. The lengths of the AH wild type and NH mutant peptide were similar.

In this model system, the structural properties can be distinguished in situ by biochemical interactions between an AH peptide and lipid molecules. After the soft adsorbed vesicle layer is formed on the gold surface, the AH peptide destabilizes the surrounding outer leaflet of the lipid bilayer, similar to the classical vesicle rupture process leading to the formation of a "rigid" bilayer on a gold substrate. To analyze this transformation, we first examined the validity of the Sauerbrey relation for both the soft and rigid layers by calculating adsorbed film thickness. While the Sauerbrey equation is still used today to estimate film thickness, more accurate models have been derived to describe the effects of adding various types of foreign masses on a quartz crystal. In order to better understand the structural transformation from a soft to a rigid film, we compared the observed changes with calculations from the Voigt−Voinova model,[34] which extends the QCM solutions beyond the Sauerbrey analogies to include viscoelastic effects. These changes were remarkably consistent over the harmonic frequencies with a film having a frequency-independent viscosity. A comparison of the mechanical loss tangent as determined by the Voigt−Voinova fit using a frequency-independent viscosity shows that the final soft vesicle layer had a tan δ greater than unity, while that of the rigid bilayer had a tan δ less

(36) Rodahl, M.; Hook, F.; Fredriksson, C.; Keller, C. A.; Krozer, A.; Brzezinski, P.; Voinova, M.; Kasemo, B. *Faraday Discuss.* **1997**, 229−246.
(37) Cho, N.-J.; Cho, S.-J.; Cheong, K.-H.; Glenn, J. S.; Frank, C. W. Manuscript in preparation.

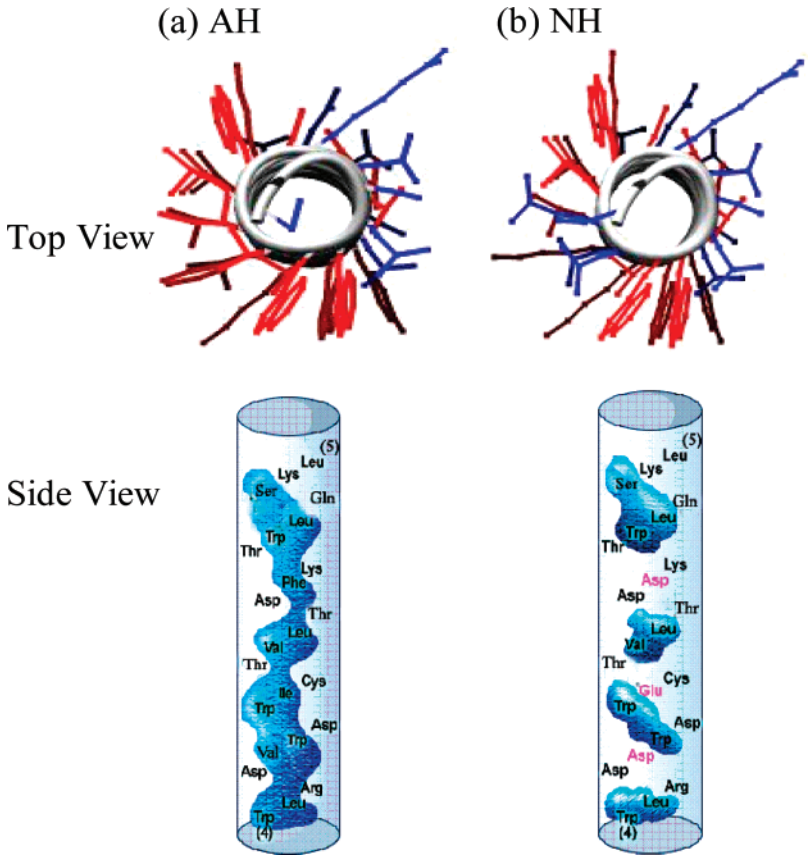

Figure 2. N-terminal amino acid sequence of amphipathic helix (AH) and nonamphipathic, nonhelical (NH) peptides. (a) The AH peptide of the hepatitis C virus (HCV) nonstructural protein NS5A with sequences GSWLRDVWDWICTVLTDFKTWLQSKLDYKD is conserved across HCV isolates. The amphipathic nature of the helix (indicated by the blue hydrophobic continuous band in side view) is conserved. (b) The NH peptide with sequences SGSWLRDDWDWECTVLTDDKTWLQSKLDYKD is synthesized by three-point mutations introduced into the AH peptide to disrupt its hydrophobic face. Three charged amino acids (pink) were spaced at intervals along the predicted N-terminal α-helix such that no sustained hydrophobic patch remained. Although this peptide is not helical, as indicated by circular dichroism measurements, we retain the same graphical plotting scheme for comparing with α-helical AH peptides.

than unity. This agrees with the notion that the soft layer is more liquid-like, while the rigid layer is solid-like.

MATERIALS AND METHODS

Materials. Small Unilamellar Vesicle Preparation. Small unilamellar vesicles of 1-palmitoyl-2-oleoyl-*sn*-glycero-3-phosphocholine (Avanti Polar Lipids) were prepared by the extrusion method. Throughout the experiments, we used a Tris buffer, 10 mM Tris (pH 7.5) and 150 mM NaCl solution with 1 mM ethylene diamine tetraacetic acid (EDTA) in 18.2 MΩ·cm MilliQ water (MilliPore). Extruded unilamellar vesicles (referred to simply as vesicles) were prepared in the following manner. Lipid films were prepared by first drying the as-supplied lipids dissolved in chloroform under a gentle stream of nitrogen at room temperature. Then the resulting lipid film was stored under vacuum for at least 5 h in order to remove residual chloroform. Multilamellar vesicles were prepared by first swelling the lipid film in aqueous solution then vortexing periodically for 5 min. The resulting multilamellar vesicles were subsequently sized by a miniextruder (Avanti Polar Lipids) through polycarbonate membranes with nominal 100-, 50-, and 30-nm pores. Vesicles were generally prepared at a nominal lipid concentration of ~5 mg·mL^{-1} and then subsequently diluted before experiments. Vesicles were generally used within 1 h of preparation.

Peptides. Amphipathic α-helical peptides and nonamphipathic nonhelical peptides were synthesized by Anaspec Corp. (San Jose, CA) (Figure 2). Whereas the AH peptide is helical with an extended hydrophobic domain (blue), NH peptides were designed to introduce three charged amino acids (pink), spaced at intervals along the predicted N-terminal-helix, such that no sustained hydrophobic patch remained. The sequences of AH and NH peptide are H-Ser-Gly-Ser-Trp-Leu-Arg-Asp-Val-Trp-Asp-Trp-Ile-Cys-Thr-Val-Leu-Thr-Asp-Phe-Lys-Thr-Trp-Leu-Gln-Ser-Lys-Leu-Asp-Tyr-Lys-Asp-NH_2 and H-Ser-Gly-Ser-Trp-Leu-Arg-Asp-***Asp***-Trp-Asp-Trp-***Glu***-Cys-Thr-Val-Leu-Thr-Asp-***Asp***-Lys-Thr-Trp-Leu-Gln-Ser-Lys-Leu-Asp-Tyr-Lys-Asp-NH_2, respectively (the introduced charged amino acids are indicated in boldface italics).

Dynamic Light Scattering (DLS). DLS was performed by a 90Plus particle size analyzer, and results were analyzed by digital autocorrelator software (Brookhaven Instruments Corp.). All measurements were taken at a scattering angle of 90° where the reflection effect is minimized. All autocorrelation functions obtained were also analyzed by CONTIN and nonnegatively constrained least-squares algorithms to check for multimodal distributions.

Quartz Crystal Microbalance Dissipation. Adsorption kinetics and the properties of the adsorbed layer were studied using a

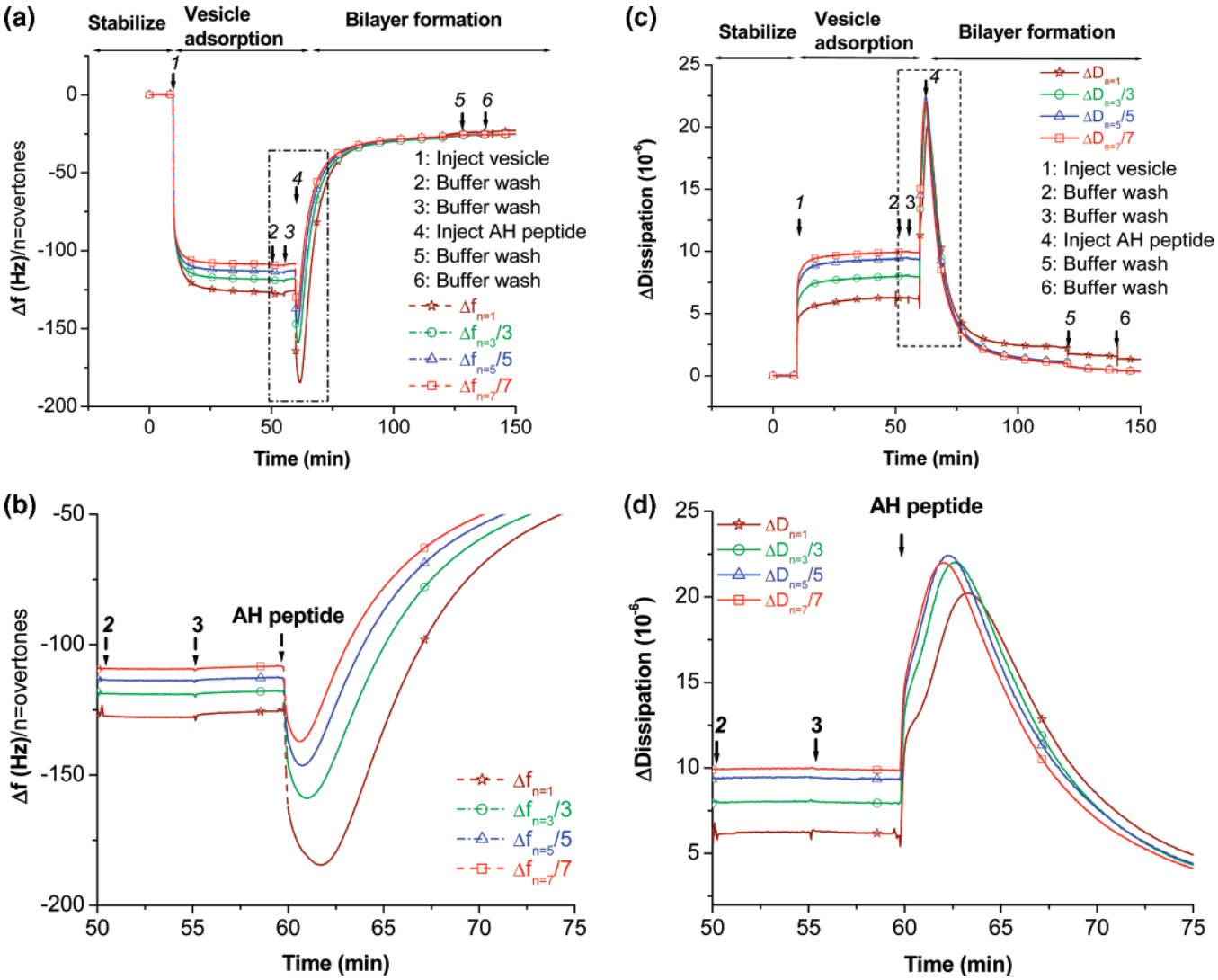

Figure 3. QCM-D responses for structural transformation from adsorbed vesicles to a bilayer induced by AH peptide. (a) QCM-D kinetic adsorption data of $\Delta f_{n=\text{overtones}}/n$ versus time for 0.01 mg·mL^{-1}vesicle with Tris buffer solution (150 mM NaCl, pH 7.5). Vesicles are added after stabilizing the frequency signal for 10 min (see arrow 1). The film was then washed twice with the same buffer (see arrows 2 and 3). Upon the addition of the AH peptide (see arrow 4), the vesicles rupture and form a bilayer on the gold surface. Two buffer washes were performed in order to ensure the stability of the film (see arrows 5 and 6). (b) Expanded view of (a). It is a detailed plot of AH peptide induced vesicle rupture process from 50 to 75 min. The markers is also presented in order to distinguish the traces of overtones (open star $\Delta f_{n=1}$, open circle $\Delta f_{n=3}$, open triangle $\Delta f_{n=5}$, and open square $\Delta f_{n=7}$ respectively. (c) Corresponding energy dissipation versus time plot demonstrates viscoelastic nature of the film changes during the structural transformation from soft vesicle layer to a rigid bilayer. (d) Expanded view of (c) to capture energy dissipation change corresponding to vesicle−AH peptide interaction.

Q-Sense D300 (Q-Sense AB, Gothenburg, Sweden) equipped with a QAFC 301 axial flow chamber. AT-cut crystals (Q-Sense) of 14 mm in diameter with 50-nm thermally evaporated gold were used for all vesicle interaction and adsorption experiments. Each QCM crystal was treated with oxygen plasma at ~80 W for ~5 min prior to measurements (March Plasmod Plasma Etcher, March Instruments). For in situ measurements, one side of the QCM was sealed with a rubber O-ring. The crystal was initially driven near its resonance frequency as indicated by a maximum in the current. To capture the characteristic dissipation, the drive circuit was short-circuited and the exponential decay of the crystal oscillation was recorded and analyzed, yielding the frequency and dissipation changes at 5, 15, 25, and 35 MHz. The temperature of the Q-Sense cell was set at 25.0°C and accurately controlled by a Peltier element in the cell with fluctuation smaller than ±0.05°C. All experiments were repeated at least three times, with a standard deviation of less than 1%.

RESULTS

Model System: Structural Transformation from Vesicles to a Bilayer via Interaction with AH Peptide. We measured the adsorption kinetics of the vesicle-to-bilayer transformation on gold surfaces using QCM-D. Characteristic results from QCM-D measurements of vesicle adsorption on a pure gold solid substrate and from the addition of an AH peptide are shown in Figure 3. The simultaneously measured changes in frequency, Δf_n, and energy dissipation, ΔD_n, obtained at four different overtones (n = 1 for the fundamental and 3, 5, and 7 for the overtones) are displayed as a function of time, where the frequency changes have been normalized by the harmonic number.

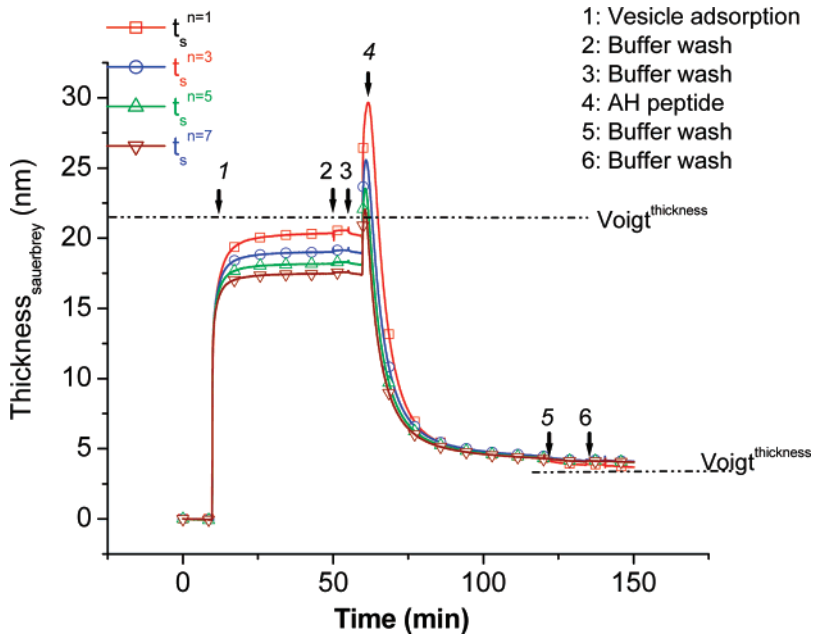

Figure 4. Model to fit experimental QCM-D data to Sauerbrey equation. Calculation of thickness using the Sauerbrey equation (eq 1) for the description of the transformation from vesicles to a bilayer. $t_s^{n=\text{overtones}}$, $n = 1$ shows fundamental overtones (open squares), $n = 3$ shows third overtones (open circles), $n = 5$ shows fifth overtones (open triangles), and $n = 7$ shows seventh overtones (opposite triangles). We added a dashed line for the thickness from the Voigt−Voinova model for both vesicle and bilayer for comparative purposes. The Voigt thicknesses for the vesicle and bilayer are 22 and 4.42 nm, respectively.

In detail, we first verified the stability of the frequency and dissipation of the bare gold crystal over a 10-min period, as shown in Figure 3 (before arrow 1). To test for the appropriateness of the Sauerbrey relation, the frequency shift values, Δf_n = overtones as shown in Figure 3a, are divided by n. Upon the addition of a vesicle solution (0.1 mg·mL^{-1}), a rapid mass uptake can be observed by a decrease in QCM-D frequency, reaching saturation at ∼-127.8, ∼-119.0, ∼-113.7, and ∼-109.36 Hz for $n = 1$, 3, 5, and 7, respectively, for the renormalized data with overtones (Figure 3b). Note that the Sauerbrey relation, eq 1, predicts that these normalized frequency changes should be independent of overtone, which is not observed experimentally. This adsorption process is accompanied by an increase in ΔD, reaching saturation at ∼6.25 × 10^{-6}, ∼8.03 × 10^{-6}, 9.47 × 10^{-6} and 9.97 × 10^{-6} for $n = 1$, 3, 5, and 7, respectively (Figure 3d). We saturated the vesicles for 40 min, and then the film was washed twice with the same buffer at 50 and 55 min to ensure the stability of the vesicle layer on the gold surface (arrows 2 and 3). Subsequently, we introduced the AH peptide (Figure 3b, d, AH peptide) and detected an initial binding and a large subsequent increase in Δf_n and decrease in ΔD_n. For the vesicles, we found that $\Delta f_n/n$ depends on the harmonic number. For 2 h, we then followed the kinetics of the resulting vesicle rupture that led to the formation of a bilayer. As the rupture process reached its culmination at $t > 125$ min, the frequencies converged to the expected value of the bilayer,[6] ∼24.9 Hz, and the dissipation approached 0.3 × 10^{-6}. As indicated in eq 1, it is clear that the normalized frequency change $\Delta f_n/n$ is independent of harmonic number for the bilayer. Our results show that we have captured two distinct regions: a soft intact vesicle layer (25 min < t < 60 min) where $\Delta f_n/n$ depends on the harmonic and a rigid bilayer ($t > 125$ min), where $\Delta f_n/n$ is now harmonic independent.

DISCUSSION

Data Analysis Using the Sauerbrey Model. We first present the measured data and discuss the frequency changes using the Sauerbrey model, showing the non-Sauerbrey behavior for soft vesicle layers that have high ΔD values. Subsequently, we compare this to the structurally transformed rigid bilayer that has low ΔD values where the behavior is properly described by the Sauerbrey equation. It is noteworthy that these two distinct regions (soft and rigid layers) provide an easy way of understanding the overall concept of full modeling using four different overtones. In order to check for the valid regions of the Sauerbrey eq 1, we utilized the frequency change data for all four overtones, as shown in Figure 3. Throughout our calculations, we assumed the density of the adlayer to be 1100 kg·m^{-3}.

The corresponding Sauerbrey thicknesses, as calculated from eq 1, are presented in Figure 4. As we anticipated for the viscoelastic soft vesicle layer, the thickness that was derived from the frequency change, reached saturation at ∼ 20.3, ∼19, ∼18.2, and ∼17.5 nm for $n = 1$, 3, 5, and 7, respectively. This analysis underestimates the thickness for all overtones compared with the Voigt-based model thickness of 22 nm (the deviation of Sauerbrey thickness for overtones are 7.7, 13.6, 17.3, and 22.45% for $n = 1$, 3, 5, and 7, respectively). The apparent decrease in the thickness of the soft layers as the overtones increase is caused by the influence of the mechanical properties of the film with increasing film thickness. The large decrease in energy dissipation upon the addition of the AH peptide (Figure 3b) is apparent evidence for a structural transformation from a dissipative soft structure to a rigid structure, as observed in our model systems. Note that there is, as expected, significantly less difference between Δf_n at the four different harmonics after the vesicle has completely ruptured, as seen in Figures 3 and 4. In addition, ΔD_n decreased and merged

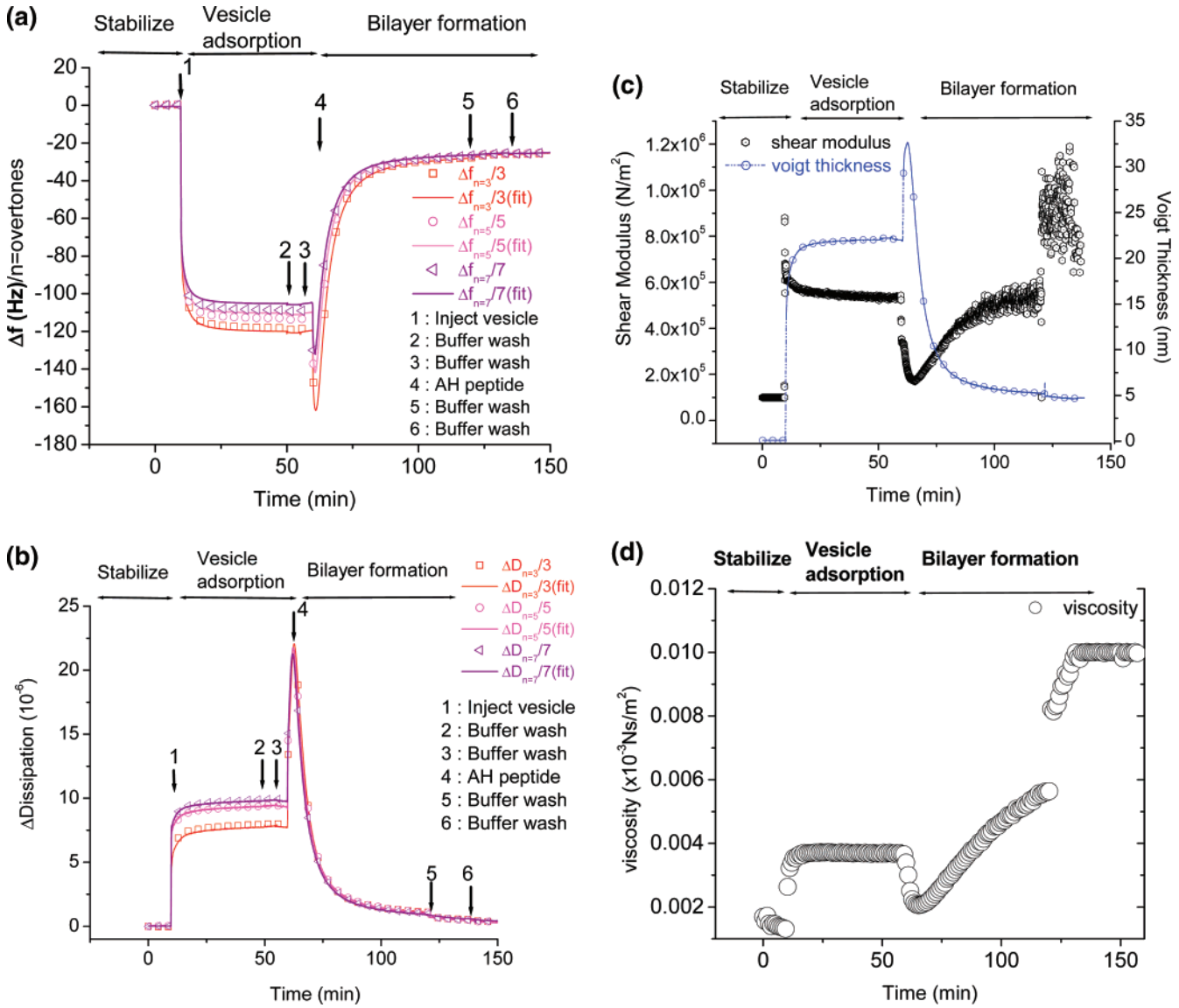

Figure 5. Model to fit experimental QCM-D data to Voigt element-based viscoelastic model. (a) Using Voigt element-based model as shown in Figure 1 to fit Δf for structural transformation from vesicles to bilayer kinetics, which demonstrates viscoelastic changes of the structural transformation from vesicle layer to bilayer. The fit between the viscoelastic model (Q-tool with density $\rho = 1100$ kg/m^3) and the experimental data are presented. (b) Corresponding ΔD fit using same model. (c) Changes in the effective shear modulus (open hexagon) and Voigt-based thickness as a function of time obtained from viscoelastic Voigt Voinova model. (d) Shear viscosity as a function of time from the viscoelastic Voigt−Voinova model.

into very small values after the vesicles ruptured. As expected, the Sauerbrey equation is an effective model for thin rigid layers.

Data Analysis Using the Voigt−Voinova Model. To better understand soft vesicle layers, we first interpreted Δf and ΔD in terms of the adsorbed mass and the structural changes in the adsorbed layer. The interpretation of viscoelastic properties of the adsorbed layer film was based on the model presented by Voinova et al.[34,38] In this model, the existence of four unknown parameters indicates that the system is undefined as long as we have only two measured quantities (Δf and ΔD at a single harmonic). However, it is possible to obtain a unique determination by using measurements of two or more harmonics.[39] It is possible to get these unique determinations only if the specific frequency dependence of the shear modulus and viscosity are assumed. In this case, both the shear modulus and viscosity are taken to be frequency independent. Since each overtone provides two experimental values (frequency and dissipation change), it is possible to uniquely determine the shear modulus and viscosity using two or more overtones.

The experimental data (open symbol) and the fit (dashed lines) using the viscoelastic model are displayed as Δf and ΔD versus time for $n = 3$, $n = 5$, and $n = 7$, as shown in Figure 5a and b. Considering the complex nature of the rupturing process, the model must be regarded as a very good fit to the measured QCM-D data even through the rupture process. At saturated coverage prior to vesicle rupturing by the AH peptide, the model fit was obtained for a film represented by an effective hydrodynamic thickness, t_{Voigt}, of 22 nm. After the rupture and transforma-

(38) Larsson, C.; Rodahl, M.; Hook, F. *Anal. Chem.* **2003**, *75*, 5080−5087.
(39) Munro, J. C.; Frank, C. W. *Macromolecules* **2004**, *37*, 925−938.

tion to a rigid bilayer, the thickness measured from the modeling decreases to 4.42 nm. These are values obtained as best fits over the whole kinetic range and may not necessarily represent the final values, which are shown in Figure 5c. In addition, we show the values of the calculated shear modului as a function of time. In the transformation from the soft vesicle layer to the rigid bilayer, both the shear modulus and the viscosity increased and the thickness decreased, which is physically reasonable. The viscosity values are shown in Figure 5d. We note here that the values for the shear modulus and viscosity after the buffer wash of the bilayer are quite uncertain because of the very small changes in dissipation that must be used to obtain those results. Voinova et al. used a ratio χ between the storage modulus μ and a loss modulus $2\pi f\eta$, which is the inverse of tan δ, to reflect the viscoelastic character, as shown in eq 4. Smaller values of tan δ characterize rigid layers, whereas larger tan δ's characterize soft layers.

White and Schrag[40] proposed a slightly different model system regarding the effect of an applied viscoelastic layer and a surrounding viscoelastic bath medium considering the effects of film thickness on the shear wavelength. They reported that frequency changes due to adsorbed layers with dissipation exceeding a critical dissipation (2×10^{-6}) were not applicable for analysis using the Sauerbrey equation. In our model framework, as one would anticipate, tan δ serves as a transition indicator between a soft and rigid layer, where soft layers are characterized by tan $\delta > 1$ and rigid layers by tan $\delta < 1$.

Data Analysis Considering the Effects of the Acoustic Wavelength and Decay Length Relative to the Film Thickness. We compared the experimental values using the Voigt−Voinova model for three different overtones. To analyze the transformation of two different regimes, we chose arbitrary saturation points for either vesicle adsorption or bilayer formation (for vesicle adsorption, $t = 59$ min; for bilayer formation, $t = 157$ min). The mechanical properties of the final film can influence the frequency and dissipation changes due to a load in a variety of ways. The frequency changes reflect the inertial changes of the load, while the dissipation changes reflect the energy losses of the load. These are both dependent on the density, shear modulus, and viscosity of the load. This dependence is not necessarily proportional to the film thickness. The details of these changes arising from the phase changes in the shear wave are determined not only by the wavelength and the penetration depth but also by the relation of these lengths to the film thickness. The film itself can become self-resonant if the fraction of the acoustic wavelength in the film approaches odd multiples of a quarter-wavelength. This would give rise not only to large additional frequency changes but also to additional large dissipation. This was demonstrated experimentally in the work of Domack.[41] As the decay length of the acoustic wave in the film decreases, the net penetration of the acoustic wave into the film decreases. In this case, the measured dissipation would be less than that of the total film.

To explore these differences, we have plotted the film thickness normalized to the shear wavelength (Figure 6a) and normalized to the decay length (Figure 6b). Two possible effects can give rise to deviations from the Sauerbrey behavior as described above.

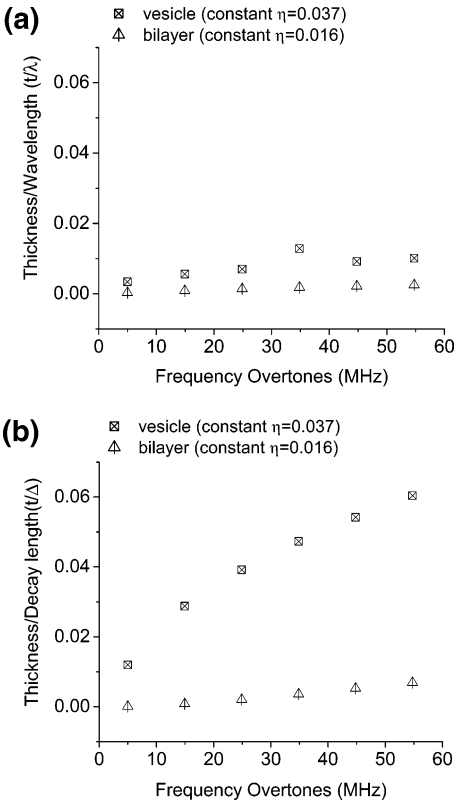

Figure 6. EM model calculations depicting the influence of wavelength and decay length on frequency overtones for two distinct regions, the soft vesicle layer and the rigid bilayer. (a) The graph represents wavelength dependence on frequency overtones up to $n = 11$ for constant viscosity. (b) The graph represented decay length dependence on frequency overtones for constant viscosity.

Table 1. Summary of the Physical Parameters from the QCM-D

		unit	soft vesicle layer	rigid bilayer
Sauerbrey thickness	f_n=1/1	m	2.03×10^{-8}	3.03×10^{-9}
	f_n=3/3	m	1.90×10^{-8}	4.46×10^{-9}
	f_n=5/5	m	1.82×10^{-8}	4.59×10^{-9}
	f_n=7/7	m	1.75×10^{-8}	4.73×10^{-9}
Voigt−Voinova thickness	t	m	2.20×10^{-8}	4.42×10^{-9}
	tanδ^b		1.165	0.34
	μ	N·m^{-2}	5.19×10^5	8.11×10^5
	η	N·s·m^{-2}	0.0037	0.01
Kanazawa thickness	t	m	20.5×10^{-8}	4.32×10^{-9}‡
EM[a]	tanδ^b		1.165	0.34
const η	μ	N·m^{-2}	5.19×10^5	8.11×10^5
	η	N·s·m^{-2}	0.0037	0.01

[a] For EM model calculation, we assumed constant viscosity over frequency overtones. [b] For the constant viscosity case, we used the fifth overtone frequency to calculate tanδ for both Voigt and EM models.

The film thickness can approach a resonance for the shear waves within the film itself ($t_f = \lambda/4, 3\lambda/4,...$) or the film thickness can rise to a measurable portion of the decay length. Figure 6a shows that the film thickness is only a very small fraction of the acoustic wavelength even at the highest overtones (less than 1%). On the other hand, Figure 6b shows that, for the vesicles, the film thickness rises to a non-negligible portion of the decay length. The influence of the harmonic frequencies is much larger for the

(40) White, C. C.; Schrag, J. L. *J. Chem. Phys.* **1999**, *111*, 11192−11206.
(41) Domack, A.; Prucker, O.; Ruhe, J.; Johannsmann, D. *Phys. Rev. E* **1997**, *56* (1), 680−689.

Table 2. Comparison of Δf and ΔD Experimental and Calculated Values

	soft vesicle layer			rigid bilayer[a]		
	measd	Voigt Voinova	Kanazawa EM[b] const η	measd	Voigt Voinova	Kanazawa EM[b] const η
Δf (Hz)						
f_n=3/3	−117.73	−121.36	−119.450	−25.143	−25.119	−25.736
f_n=5/5	−112.59	−112.08	−109.780	−24.802	−24.902	−25.184
f_n=7/7	−108.3	−104.79	−103.481	−24.843	−26.483	−25.941
ΔD (10^{-6})						
$D_{n=3}$	7.932	7.4111	7.640	0.356	0.378	0.512
$D_{n=5}$	9.362	9.3703	9.190	0.328	0.366	0.441
$D_{n=7}$	9.874	9.7269	9.240	0.337	0.294	0.367

[a] In order to compare the calculation values from the experiment with those from the model, we chose saturation points for two distinct regions. (i.e., "soft" vesicle layer t = 59 min, rigid bilayer t = 157 min). [b] For EM model$_a$ calculation, we assumed constant viscosity over frequency overtones.

vesicles than for the bilayer. The thickness, as normalized to the decay length, shows a very significant change (500%) with increasing harmonic frequency. These results suggest that the large decay length in the vesicles relative to the vesicle size is closely related to the failure of the Sauerbrey relation.

Summary Tables. Table 1 summarizes all the experimental QCM-D results and compares those obtained from the Voigt−Voinova[34] model. We also included the calculations from the EM model using the assumption of a frequency-independent viscosity. In this study, two distinct mechanical layers, soft intact vesicle layers and a rigid bilayer, were examined in order to verify the viscoelastic character of the distinct layers. Soft intact vesicle layers occur with higher values of average thickness than a rigid bilayer. Using Sauerbrey thickness for density, 1100 kg·m^{-3}, the deviation for the thickness of soft vesicle layers is 7.72, 13.63, 17.27, and 20.45%, respectively, for the first, third, fifth, and seventh frequency overtones as shown in the first four rows. It is noteworthy that, when applying the Sauerbrey equation to convert the frequency changes to thickness, the Sauerbrey thickness decreases as the harmonic number increases. In the case of a frequency dependence in Δf or a large energy dissipation ΔD measured at multiple harmonics, all these effects are general and may be important when considering other flexible macromolecules in the adsorbed state. The thickness values using the Voigt−Voinova model are shown in row 5. In the case of a rigid bilayer, the deviation is less than 1% for all overtones. At saturated coverage prior to vesicle rupturing by the AH peptide, the model fit was obtained for a film represented by an effective hydrodynamic thickness, t_{Voigt}, of 2.2×10^{-8} m, $\mu_f = 5.19 \times 10^5$ N·m^{-2}, and $\eta_f = 3.70 \times 10^{-3}$ N·s·m^{-2} using $\rho_f = 1.1 \times 10^3$ kg·m^{-3}. Values comparable to the Voigt−Voinova model cited in rows 5, 6, 7, and 8 and shown for the EM model (in rows 9, 10, 11, and 12). Note that the Voigt−Voinova and EM models use a constant viscosity in order to yield the same information. This agreement shows that the calculation from the Voigt−Voinova model is quite accurate. After the rupture and transformation of the soft vesicles to a rigid bilayer, the thickness determined from the modeling decreased to 4.42 nm, $\mu_f = 8.11 \times 10^5$ N·m^{-2} and $\eta_f = 10 \times 10^{-3}$ N·s·m^{-2}. The model fit presented as the soft vesicle layer transformed into a rigid bilayer; both the shear modulus and viscosity increased, and the thickness decreased.

In Table 2, we compared the predicted values of the normalized frequency changes and the dissipation changes using the Voigt−Voinova model and the EM models at three of the overtones (3, 5, 7). For soft vesicle adsorption layers, we could examine the frequency deviation upon changes of frequency overtones up to 20%. However, in the case of the rigid lipid bilayer, frequency changes do not depend on the frequency overtones. We used both the Voigt−Voinova and EM models to calculate the frequency and dissipation changes under the condition of an assumed frequency-independent viscosity.

CONCLUSION

In this paper, we have presented a model system that contains two distinct properties of layers. One is the soft adsorbed vesicle layer, which does not follow the general Sauerbrey relation; the other is the rigid bilayer, transformed from soft vesicle layers, which agrees with the Sauerbrey equation. Soft vesicle layers have lower viscosity and shear modulus compared with a transformed rigid bilayer due to structural alterations. This study confirms both the validity and limitations of the Sauerbrey equation. One of the limitations of the Sauerbrey equation is that it underestimates the thickness for multiple harmonics in the case of higher dissipation. Because of the complexity of the biomembrane, which contains various proteinaceous components, there is a clear need to understand model systems, where they are subjected to higher dissipation. While using a wide range of available surface-sensitive techniques to study natural biological systems, we should distinguish physical properties of layers in order to apply the proper model.

Received for review May 10, 2007. Accepted June 25, 2007.

AC0709504